

# Design of a Breast Phantom for Quantitative MRI

Kathryn E. Keenan PhD,<sup>1\*</sup> Lisa J. Wilmes PhD,<sup>2</sup> Sheye O. Aliu PhD,<sup>2</sup>  
David C. Newitt PhD,<sup>2</sup> Ella F. Jones PhD,<sup>2</sup> Michael A. Boss PhD,<sup>1</sup>  
Karl F. Stupic PhD,<sup>1</sup> Stephen E. Russek PhD,<sup>1</sup> and Nola M. Hylton PhD<sup>2</sup>

**Purpose:** We present a breast phantom designed to enable quantitative assessment of measurements of  $T_1$  relaxation time, apparent diffusion coefficient (ADC), and other attributes of breast tissue, with long-term support from a national metrology institute.

**Materials and Methods:** A breast phantom was created with two independent, interchangeable units for diffusion and  $T_1/T_2$  relaxation, each with flexible outer shells. The  $T_1$  unit was filled with corn syrup solution and grapeseed oil to mimic the relaxation behavior of fibroglandular and fatty tissues, respectively. The diffusion unit contains plastic tubes filled with aqueous solutions of polyvinylpyrrolidone (PVP) to modulate the ADC. The phantom was imaged at 1.5T and 3.0T using magnetic resonance imaging (MRI) scanners and common breast coils from multiple manufacturers to assess  $T_1$  and  $T_2$  relaxation time and ADC values.

**Results:** The fibroglandular mimic exhibited target  $T_1$  values on 1.5T and 3.0T clinical systems (25–75 percentile range: 1289 to 1400 msec and 1533 to 1845 msec, respectively) across all bore temperatures. PVP solutions mimicked the range of ADC values from malignant tumors to normal breast tissue (40% PVP median:  $633 \times 10^{-6} \text{ mm}^2/\text{s}$  to 0% PVP median:  $2231 \times 10^{-6} \text{ mm}^2/\text{s}$ ) at temperatures of 17–24°C. The interchangeable phantom units allowed both the diffusion and  $T_1/T_2$  units to be tested on the left and right sides of the coil to assess any variation.

**Conclusion:** This phantom enables  $T_1$  and ADC measurements, fits in a variety of clinical breast coils, and can serve as a quality control tool to facilitate the standardization of quantitative measurements for breast MRI.

J. MAGN. RESON. IMAGING 2016;00:000–000.

Breast cancer is one of the three most common cancers in women and the second leading cause of cancer deaths in women in 2014.<sup>1</sup> Magnetic resonance imaging (MRI) with quantitative sequences is increasingly employed for breast cancer diagnosis, staging, and monitoring. Several clinical trials that use these MRI techniques to assess treatment are currently underway.<sup>2,3</sup>

To assess the efficacy of breast cancer treatment, it is clinically important to understand the sources of variability in breast MRI, such as fat suppression, variations in the left and right sides of the coil, and image distortion, so that observed changes in patients can be interpreted correctly. Breast MRI measurements, particularly those used in multicenter treatment trials, should be standardized using reliable methods for quality control. In fact, standardized acquisition parameters, quality control protocols, and data reporting

have been previously recommended.<sup>4</sup> In addition, a critical step toward image quality assurance is through the use of a standard reference object or phantom.

An ideal breast phantom should have the following attributes: 1) ability to simulate the heterogeneous distribution of fat and fibroglandular tissue in the breast to test fat suppression techniques; 2) design for quantitatively evaluating standard proton spin relaxation time ( $T_1$ ,  $T_2$ ), and diffusion protocols in breast MRI; 3) compatibility with commonly used breast coil types; 4) ability to assess variation in the left and right sides of the coil; and 5) ability to measure image distortion.<sup>5</sup> In an effort to develop a new breast phantom, we evaluated phantoms presented in the literature. We found that these phantoms were either incompatible with some breast coil types,<sup>6</sup> or unable to assess diffusion MRI.<sup>7</sup>

View this article online at [wileyonlinelibrary.com](http://wileyonlinelibrary.com). DOI: 10.1002/jmri.25214

Received Nov 30, 2015, Accepted for publication Feb 12, 2016.

\*Address reprint requests to: K.K., 325 Broadway, Boulder, CO 80305. E-mail: [kathryn.keenan@nist.gov](mailto:kathryn.keenan@nist.gov)

From the <sup>1</sup>Physical Measurement Laboratory, National Institute of Standards and Technology, Boulder, Colorado, USA; and <sup>2</sup>Department of Radiology and Biomedical Imaging, University of California, San Francisco, California, USA

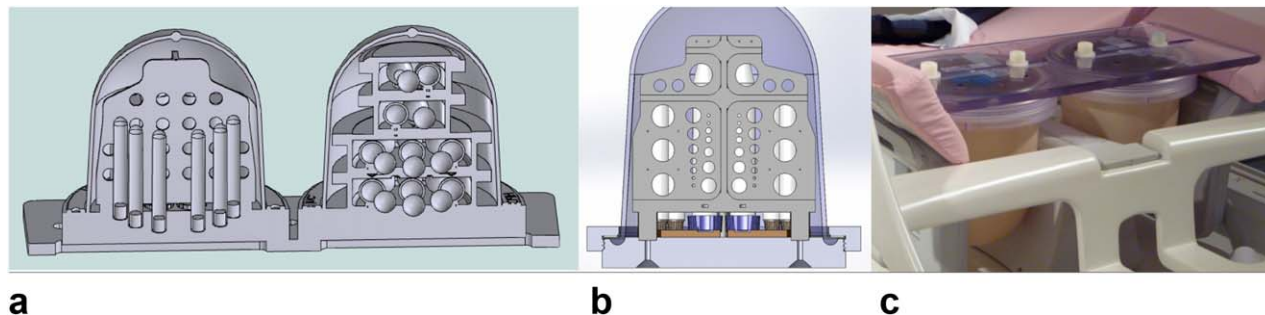


**FIGURE 1:** Breast phantom model (A) with the diffusion phantom unit and geometric distortion array on the left and  $T_1/T_2$  phantom unit on the right. (B) Detail of the resolution plate. Photo of prototype (C) prepared for imaging in a dedicated breast MR coil. The breast phantom is compatible with multiple breast coil designs and is able to assess diffusion MRI, which are improvements over previous phantoms.

In this work we present a new breast phantom that is designed and fabricated to enable quantitative assessment of measurements of  $T_1$  relaxation time, apparent diffusion coefficient (ADC), and other attributes of breast tissue, with long-term support from a national metrology institute.

**Materials and Methods**

**Phantom Design**

The initial phantom prototype was guided by several design elements: 1) interspersed fibroglandular and adipose breast tissue elements extending over anatomically representative distances in the anterior–posterior, superior–inferior, and medial–lateral directions to test fat suppression techniques; 2) adherence to in vivo physiologic ranges for both  $T_1$  relaxation and ADC values; 3) physical compatibility with commonly used clinical breast MRI coils; 4) repeated elements in both the left and right sides of the coil; and 5) geometric structures for measuring image distortion.

The breast phantom was created as two distinct, interchangeable units: one for diffusion and geometric distortion evaluation and one for  $T_1/T_2$  relaxation evaluation, which are connected via a polycarbonate “backboard” (Fig. 1). Both phantom units consist of a flexible outer silicone shell (Durometer 10A, dimensions: 15.0 cm height and 12.5 cm diameter) to allow easy positioning in many coil geometries, and rigid polycarbonate internal components to ensure precise geometry and separation between materials. The interchangeable nature allows the phantom units to be imaged in both the left and right sides of a typical clinical breast coil. The polycarbonate backboard ensures rigid, reproducible spacing between the two breast phantom units, and it allows the phantom unit position to be adjusted in the medial–lateral plane for a better fit in breast coils.

In vivo measurements of the  $T_1$  and  $T_2$  relaxation times and ADC properties of fibroglandular, adipose, benign tumor, and malignant tumor tissues were compiled from the literature and are given in Table 1.<sup>8–11</sup> To mimic the  $T_1$  relaxation time of

**TABLE 1. Target In Vivo Breast Relaxation Times and Apparent Diffusion Coefficient Values, Compiled From the Literature**

	1.5T		3.0T		Apparent diffusion coefficient $\pm$ SD ( $10^{-6}$ mm <sup>2</sup> /s)
	$T_1$ relaxation time $\pm$ SD (msec)	$T_2$ relaxation time $\pm$ SD (msec)	$T_1$ relaxation time $\pm$ SD (msec)	$T_2$ relaxation time $\pm$ SD (msec)	
Adipose tissue	296.01 $\pm$ 12.94 <sup>a</sup> 264.62 $\pm$ 2.38 <sup>b</sup>	53.33 $\pm$ 2.11 <sup>a</sup> 57.63 $\pm$ 1.36 <sup>b</sup>	366.78 $\pm$ 7.75 <sup>a</sup>	52.96 $\pm$ 1.54 <sup>a</sup>	
Fibroglandular tissue	1266.18 $\pm$ 81.8 <sup>a</sup> 795.64 $\pm$ 21.12 <sup>b</sup>	57.51 $\pm$ 10.15 <sup>a</sup> 62.82 $\pm$ 4.06 <sup>b</sup>	1444.83 $\pm$ 92.7 <sup>a</sup>	54.36 $\pm$ 9.35 <sup>a</sup>	1950 $\pm$ 380 <sup>d</sup>
Benign mass mimic	1049.02 $\pm$ 40.31 <sup>b</sup>	89.15 $\pm$ 8.33 <sup>b</sup>			1740 $\pm$ 460 <sup>d</sup>
Benign lesion mimic					1610 $\pm$ 330 <sup>d</sup>
Malignant lesion mimic					1410 $\pm$ 220 <sup>d</sup>
Malignant mass mimic	876.09 $\pm$ 27.83 <sup>b</sup>	74.76 $\pm$ 3.90 <sup>b</sup>			1250 $\pm$ 290 <sup>d</sup>

<sup>a</sup>Rakow-Penner et al. in vivo measurements (10).  
<sup>b</sup>Merchant et al. in vivo measurements (8).  
<sup>c</sup>Partridge et al. in vivo measurements (9).  
<sup>d</sup>Partridge et al. in vivo measurements (11).

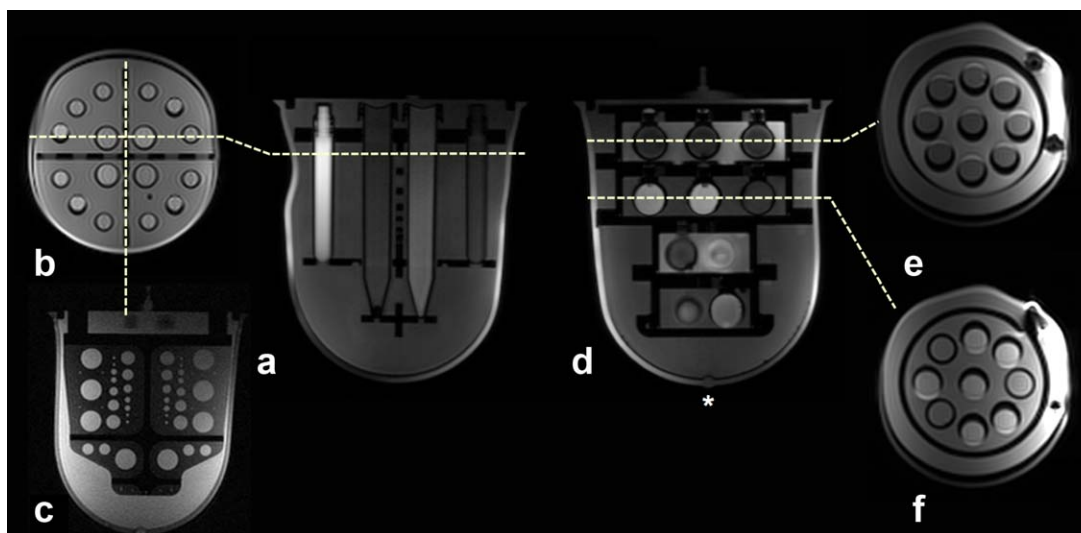


**FIGURE 2:** Diffusion phantom axial (A) and coronal (B)  $T_1$ -weighted images of the breast phantom prototype and resolution plate (C).  $T_1/T_2$  relaxation phantom axial (D) and coronal images of layer 1 (E) and layer 2 (F). Layer 1 (E) contains grapeseed oil bulk solution, and layer 2 (F) contains fibroglandular tissue mimic solution. The nipple mimic is denoted with \*. The flexible outer shell allowed some deformation to accommodate coil geometries, but did not affect positioning of the internal elements.

fibroglandular tissue, the bulk solution is 35% weight-by-weight (w/w) corn syrup (ACH Food Companies, Cordova, TN) in deionized water. Grapeseed oil (Sovena USA, Rome, NY) was used to mimic both the chemical shift from water and the  $T_1$  and  $T_2$  relaxation times of adipose tissue in the breast. Polyvinylpyrrolidone (PVP, average mol. wt. 40,000 Da, Sigma-Aldrich, St. Louis, MO) was used to control the diffusion of water.<sup>12,13</sup> PVP concentrations of 0, 10, 14, 18, 25, and 40% w/w were included to mimic the diffusion properties of fibroglandular and tumor tissues (Table 1) at bore temperature. The 10, 14, and 18% w/w PVP tubes were for determination of ADC measurement resolution, to decipher the sensitivity of ADC measurements to distinguish benign and malignant lesions. The differences between the expected ADC values of 10 and 18% w/w PVP are similar to the differences between benign and malignant tumors:  $1610 \pm 330 \times 10^{-6} \text{ mm}^2/\text{s}$  compared to  $1250 \pm 290 \times 10^{-6} \text{ mm}^2/\text{s}$ .<sup>9</sup>

The diffusion phantom unit, shown in Fig. 2A–C, contains 16 plastic sample tubes (4 large, 12 small), aligned in the anterior–posterior direction, containing the PVP solutions. Adipose tissue mimic tubes were also included to test the efficacy of fat suppression techniques in ADC sequences. The large tubes in the diffusion phantom unit measure 12.5 cm long and 1.4 cm inner diameter (Falcon 15 mL Conical Tube); the small tubes were 8.7 cm long and 1.0 cm in outer diameter (Wheaton 5 mL Int RB CryoElite Tube). The diffusion phantom unit also contains two perpendicular polycarbonate plates, bisecting the phantom in the axial and sagittal orientations that are designed for assessing image distortions and resolution, respectively. The axial plate contains a grid of circles on 2.0 cm center-to-center spacing in both the anterior–posterior and right–left directions, with four anterior–posterior rows of four to six, 1.0-cm diameter circles (Fig. 1A). The sagittal plate contains circular features with diameters ranging from 0.1 cm to 1.5 cm that can be used to measure resolution accuracy (Figs. 1B, 2C).

The  $T_1$  relaxation phantom unit as shown in Fig. 2D–F consists of four closed cylindrical compartments, alternately filled with

adipose or fibroglandular tissue mimics.<sup>14</sup> Each compartment contains a layer of polypropylene spheres (1.8 cm inner diameter), filled with a variety of tissue mimics described in Table 2. The two larger, more posterior layers each contain nine internal spheres (Fig. 2E,F), and the two smaller, anterior layers each contain three internal spheres.

### Reference Measurements

The  $T_1$  and diffusion phantom units were imaged on a small-bore 1.5T preclinical MRI system (Agilent Technologies, Santa Clara, CA) to generate reference values and to measure the effect of temperature on the  $T_1$ ,  $T_2$ , and ADC of the different mimic materials. Components were imaged at clinically relevant bore temperatures: 17.91, 19.07, 20.16, and 22.11°C ( $\pm 0.01^\circ\text{C}$ ). The temperature control setup consisted of two concentric cylinders with an outer fill of proton-MR invisible solution (Fluorinert FC-43, 3M, St. Paul, MN) and an inner fill of deionized water. Samples were placed in the inner compartment. The outer compartment was connected to a temperature-controlled circulator (PolyScience 9102, Niles, IL), which was filled with Fluorinert. The temperature change in the inner compartment is driven by the change in the Fluorinert that is circulating in the outer fill. Temperature was measured continuously using an MRI-compatible fiberoptic probe (OTP-M, OpSens, Québec, Canada) located centrally in the inner compartment.  $T_1$  relaxation time was measured using a spin-echo inversion recovery (IR) sequence with repetition time / echo time (TR/TE) 10,000/14.75 msec and inversion times (TI) 50, 75, 100, 125, 150, 250, 500, 1000, 1500, 2000, and 3000 msec.  $T_2$  relaxation time was measured using a spin-echo multiple echo time sequence with TR 5000 msec and echo times 15, 20, 40, 80, 160, 320, and 640 msec. ADC was measured using a spin-echo sequence with TR/TE 10,000/33.64 msec and b-values 0, 100, 600, and 900  $\text{s}/\text{mm}^2$ . For all experiments the field of view (FOV) was  $150 \text{ mm}^2$ , and matrix size was  $256 \times 256$ . Quantitative analysis to determine  $T_1$ ,  $T_2$ , and ADC was performed using software

TABLE 2. 1.5T MRI Measured Properties of the Phantom Components

	Material components	Temperature (°C)	T <sub>1</sub> relaxation time ± SD (msec)	T <sub>2</sub> relaxation time ± SD (msec)	Apparent diffusion coefficient ± SD (10 <sup>-6</sup> mm <sup>2</sup> /s)
Fibroglandular tissue mimic	35% Corn syrup w/w in water	17.91	1096.65 ± 6.35	236.33 ± 6.97	966 ± 5
		19.07	1115.53 ± 9.95	236.43 ± 2.13	1013 ± 21
		20.16	1151.58 ± 9.81	241.38 ± 8.99	1030 ± 7
		22.11	1200.15 ± 8.57	262.18 ± 6.77	1084 ± 10
Adipose tissue T <sub>1</sub> and spectral shift mimic	Grapeseed oil: Chemical shift from water 3.10 ppm	17.91	227.45 ± 2.13	41.30 ± 1.11	
		19.07	230.48 ± 2.31	42.30 ± 1.95	
		20.16	238.63 ± 4.01	42.40 ± 1.59	
		22.11	249.28 ± 4.64	43.93 ± 1.67	
Diffusion mimics: Benign lesion	10% PVP w/w in water	17.91	2015.25 ± 24.80		1536 ± 7
		19.07	2026.73 ± 24.66		1627 ± 25
		20.16	2127.95 ± 39.20		1630 ± 12
		22.11	2172.60 ± 65.13		1714 ± 6
Malignant lesion	14% PVP	17.91	1720.70 ± 18.12		1348 ± 4
		19.07	1732.00 ± 12.98		1407 ± 7
		20.16	1817.83 ± 10.82		1439 ± 11
		22.11	1903.15 ± 22.23		1522 ± 6
Malignant mass	18% PVP	17.91	1490.53 ± 20.42		1238 ± 9
		19.07	1518.93 ± 28.02		1307 ± 15
		20.16	1628.23 ± 13.26		1318 ± 8
		22.11	1704.85 ± 24.43		1389 ± 7
	25% PVP	17.91	1050.55 ± 6.80		861 ± 12
		19.07	1073.35 ± 9.20		907 ± 15
		20.16	1125.88 ± 15.28		927 ± 9
		22.11	1182.48 ± 8.05		983 ± 12
	40% PVP	17.91	630.30 ± 1.61		557 ± 9
		19.07	651.97 ± 6.88		600 ± 17
		20.16	681.53 ± 3.33		602 ± 10
		22.11	723.97 ± 16.68		640 ± 9

All measurements were made on a 1.5T small-bore MRI system using spin-echo sequences, specifically: inversion recovery method to measure T<sub>1</sub>, variable echo for T<sub>2</sub>, and three gradient directions with b-values of 0, 100, 600, and 900 s/mm<sup>2</sup> for ADC measurements. Determination of standard deviation is described in the Materials and Methods.

(PhantomViewer) developed at the National Institute of Standards and Technology<sup>14</sup> using standard python toolboxes including LMFIT.<sup>15</sup> Mean and standard deviation of the model fit are reported.

Phantom mimic solutions were also assessed at 3.0T using a nuclear magnetic resonance (NMR) spectrometer. Aliquots of each solution were transferred into standard 5 mm NMR tubes. A fiber optic temperature probe was positioned in each NMR tube so that the sensing element was in the middle of the RF coil. Each sample was equilibrated to 20.00°C (standard deviation  $\pm 0.03^\circ\text{C}$ ) for at least 15 minutes and was continuously monitored during the acquisition of relaxometry data.

Inversion recovery and Carr-Purcell-Meiboom-Gill (CPMG) experiments were performed to measure  $T_1$  and  $T_2$  relaxation times, respectively.<sup>16,17</sup> Each experiment sampled 20 different inversion/decay times. TI ranged from 0.005 to 15 seconds, and the nominal  $\tau_{cp}$ , the time from a  $180^\circ$  refocusing pulse to the resultant echo, was 1 msec. The maximum length of the Carr-Purcell echo train varied according to the sample, but ranged from 0.486 to 20.3 seconds. Time-domain data were Fourier transformed, the areas of the resonance peaks were plotted as a function of TI or echo train duration, and fit to exponential recovery and decay curves, respectively.

A spin-echo sequence was performed on the adipose and fibroglandular tissue mimic to replicate the  $T_2$  measurements made on the 1.5T preclinical MRI system. Single echoes were acquired with a variable TE starting at 15 msec and increasing in 15-msec increments to 195 msec. Initial amplitude of the free induction decay was plotted as a function of TE and fit to an exponential decay.

### Clinical Imaging Techniques

$T_1$ ,  $T_2$  relaxation times and ADC values of the phantom components were measured on commercially available systems at 1.5T (Signa, GE Healthcare, Milwaukee, WI) using an open, bilateral, 8-channel breast coil (Hologic (formerly Sentinelle Medical), Toronto, Ontario, Canada), and at 3.0T (Verio, Siemens Medical Solutions, Erlangen, Germany) using an open, bilateral, 16-channel breast coil (Hologic). All imaging was done in the axial orientation.  $T_1$  relaxation measurements were made using 3D variable flip angle (VFA) methods with flip angles: 5, 8, 15, 22, and  $43^\circ$ . At 1.5T, TR/TE was 16.7/4.0 msec with 2 averages, slice thickness 2 mm, FOV 400 mm<sup>2</sup>, and pixel size 1.56 mm<sup>2</sup>. At 3.0T, TR/TE was 16.0/2.6 msec with 1 average, slice thickness 1 mm, FOV 340 mm<sup>2</sup> and pixel size 0.89 mm<sup>2</sup>.  $T_2$  relaxation measurements were made using 2D variable echo time (VTE) methods using the same slice thickness and spatial resolution as the  $T_1$  VFA measurements. At 1.5T, TR was 2000 msec, and the echo times were 8.34, 16.68, 25.03, 33.37, 41.72, 50.06, 58.40, and 66.75 msec. At 3.0T, TR was 4000 msec, and the echo times were 11.6, 23.2, 34.8, 46.4, 58.0, 69.6, 81.2, and 92.8 msec. ADC measurements were performed using single-shot echo-planar imaging (EPI) and four b-values: 0, 100, 600, and 800 s/mm<sup>2</sup>, with anterior/posterior frequency-encode direction and bandwidth 1953 Hz. At 1.5T, TR/TE was 7500/70.4 msec, slice thickness 2 mm, FOV 400 mm<sup>2</sup>, and pixel size 1.56 mm<sup>2</sup>. At 3.0T, TR/TE was 14100/88 msec, slice thickness 2 mm, FOV 399 mm<sup>2</sup>, and pixel size 2.63 mm<sup>2</sup>.

### Clinical Image Analysis

Clinical image analysis consisted of the creation of image maps and selection of the regions of interest (ROIs). We used software developed in the IDL programming environment (Exelis Visual Information Solutions, Boulder, CO) at the University of California San Francisco.<sup>18</sup> To allow for better visualization and to ensure that ROIs could be drawn on a sufficient number of slices, axial images were interpolated in the slice direction to yield isotropic voxels and then resampled to the coronal orientation. Interpolation and resampling were not necessary for diffusion-weighted images, because the tubes in the diffusion phantom unit were sufficiently visible in the original axial orientation.

$T_1$  maps for VFA acquisitions were computed using the method for spoiled gradient steady state acquisitions.<sup>19,20</sup> In brief, the signal  $S_i$  acquired at a flip angle  $\alpha_i$  is a function of the  $T_1$ , TR, and equilibrium magnetization,  $M_0$ :

$$S_i = M_0 \sin \alpha_i \frac{1 - E_1}{1 - \cos \alpha_i E_1} \quad (1)$$

where  $E_1 = e^{-TR/T_1}$ . Since signal is acquired at different flip angles, the  $T_1$  can be determined by transforming the VFA signal equation into the linear form  $Y_i = mX_i + b$ ,

$$\frac{S_i}{\sin \alpha_i} = E_1 \frac{S_i}{\tan \alpha_i} + M_0(1 - E_1) \quad (2)$$

and then extracting  $T_1$  from the slope  $m = E_1$  as follows<sup>19,20</sup>:

$$T_1 = -\frac{TR}{\ln(m)} \quad (3)$$

Voxels with nonphysiological  $T_1$  values (less than 0 or greater than 10 sec) were excluded prior to computing summary statistics (mean, median, etc.). ADC maps were generated by fitting the equation:

$$\ln S_b = \ln S_0 - bADC \quad (4)$$

using a linear least-squares approach, where  $S_b$  and  $S_0$  are the diffusion-weighted and nondiffusion-weighted signals, respectively, and  $b$  is the diffusion sensitizing factor.

ROIs were created manually. For each of the four layers of the  $T_1$  phantom unit, a 10 mm diameter circle (approximated as a polygon with 24 vertices) was placed within each sphere on the five contiguous slices centered on the slice with the greatest cross-sectional area for that sphere. All five such 2D ROIs were then stacked into a multislice, cylindrical ROI. Multislice ROIs were similarly generated for the background of all four layers. ROIs for the background were identical to ROIs for the spheres in shape and size and were drawn on the same slices as the spheres' ROIs.

ROIs for the diffusion phantom unit were rectangles measuring  $\sim 70$  mm by 3 mm for the four large tubes and 55 mm by 2 mm for the 12 small tubes. ROIs for the large tubes were created on the three contiguous slices centered on the slice with the greatest cross-sectional area of the tubes, while ROIs for the smaller tubes were created on the two contiguous slices with the greatest cross-sectional area of the tubes in each slice. These 2D ROIs were

**TABLE 3. 3.0T NMR Measured Properties of the Phantom Components at 20°C**

	Material components	T <sub>1</sub> relaxation time (msec)	T <sub>2</sub> relaxation time (msec)
Fibroglandular tissue mimic <sup>a</sup>	35% Corn syrup w/w in water	1230 ± 34.6	47.3 ± 0.9
Adipose tissue T <sub>1</sub> and spectral shift mimic <sup>a</sup>	Grapeseed oil	297 ± 6.3	32.5 ± 1.1
Diffusion mimics <sup>b</sup> Benign lesion	10% PVP w/w in water	2300 ± 5.2	1953.1 ± 0.9
Malignant lesion	14% PVP	2010 ± 3.8	1692 ± 1.3
Malignant mass	18% PVP	1770 ± 3.4	1479.3 ± 0.9
	25% PVP	1200 ± 3.4	1017.3 ± 0.8
	40% PVP	714 ± 1.7	584.8 ± 0.2

<sup>a</sup>T<sub>2</sub> measurements made using spin-echo technique; details in the Materials and Methods section.  
<sup>b</sup>T<sub>2</sub> measurements made using CPMG technique; details in the Materials and Methods section.

subsequently stacked into multislice, rectangular cuboid ROIs. In some datasets, the geometry of the tubes was distorted due to EPI artifacts. For those datasets, ROIs were rotated at angles ranging from -5 to +5 degrees to ensure that the ROIs were circumscribed within the tubes.

To assess geometric distortion, we defined each hole based on pixel intensity, calculated the center of each defined hole, and measured center-to-center distances between all holes in the right/left (R/L) and anterior/posterior (A/P) directions. We report the average center-to-center distance across a row or column.

## Results

### Phantom Design and Tissue Mimics

The small-bore MRI and NMR spectrometer measurements revealed that the fibroglandular mimic material (35% corn syrup by mass water) was within the range of in vivo T<sub>1</sub> values from the literature<sup>10</sup> at 1.5T and 3.0T, but the T<sub>2</sub> relaxation time measured at 1.5T was more than four times longer than the targeted in vivo T<sub>2</sub> (Tables 1–3).

For an adipose tissue mimic, grapeseed oil possessed an ideal combination of T<sub>1</sub> and T<sub>2</sub> relaxation times along with an appropriate chemical shift (Tables 2 and 3). Using a spectral fat suppression method, signal from the grapeseed oil and the silicone outer shell were suppressed when compared to corresponding T<sub>1</sub>-weighted images acquired without fat suppression (Fig. 3).

The measured ADC values for the PVP samples included in the breast diffusion phantom unit spanned the literature-reported range of ADC values for malignant and benign breast masses and lesions as well as for normal tissue (Table 2).<sup>9</sup>

The interchangeable phantom units allow both the diffusion and T<sub>1</sub>/T<sub>2</sub> unit to be tested on the left and right

sides of the coil to assess any variation. The flexible silicone outer shell allowed the phantom units to easily fit into the commonly used, commercially available breast coils that were tested.

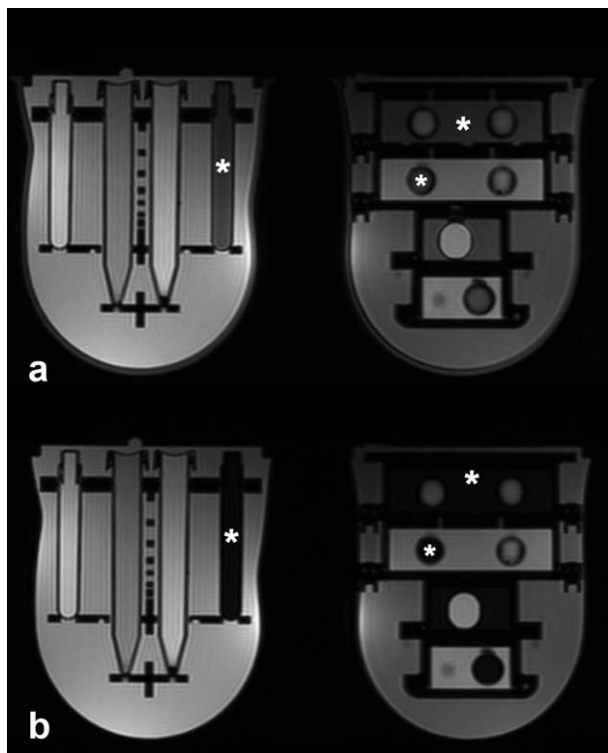


**FIGURE 3:** Axial T<sub>2</sub>-weighted images acquired without (A) and with (B) spectral fat suppression demonstrate that fat signal is suppressed in the adipose tissue mimic (locations of adipose tissue mimic noted with \*). Additionally, signal from the silicone shell, at the boundary of the breast phantom, is suppressed using spectral suppression techniques (B).

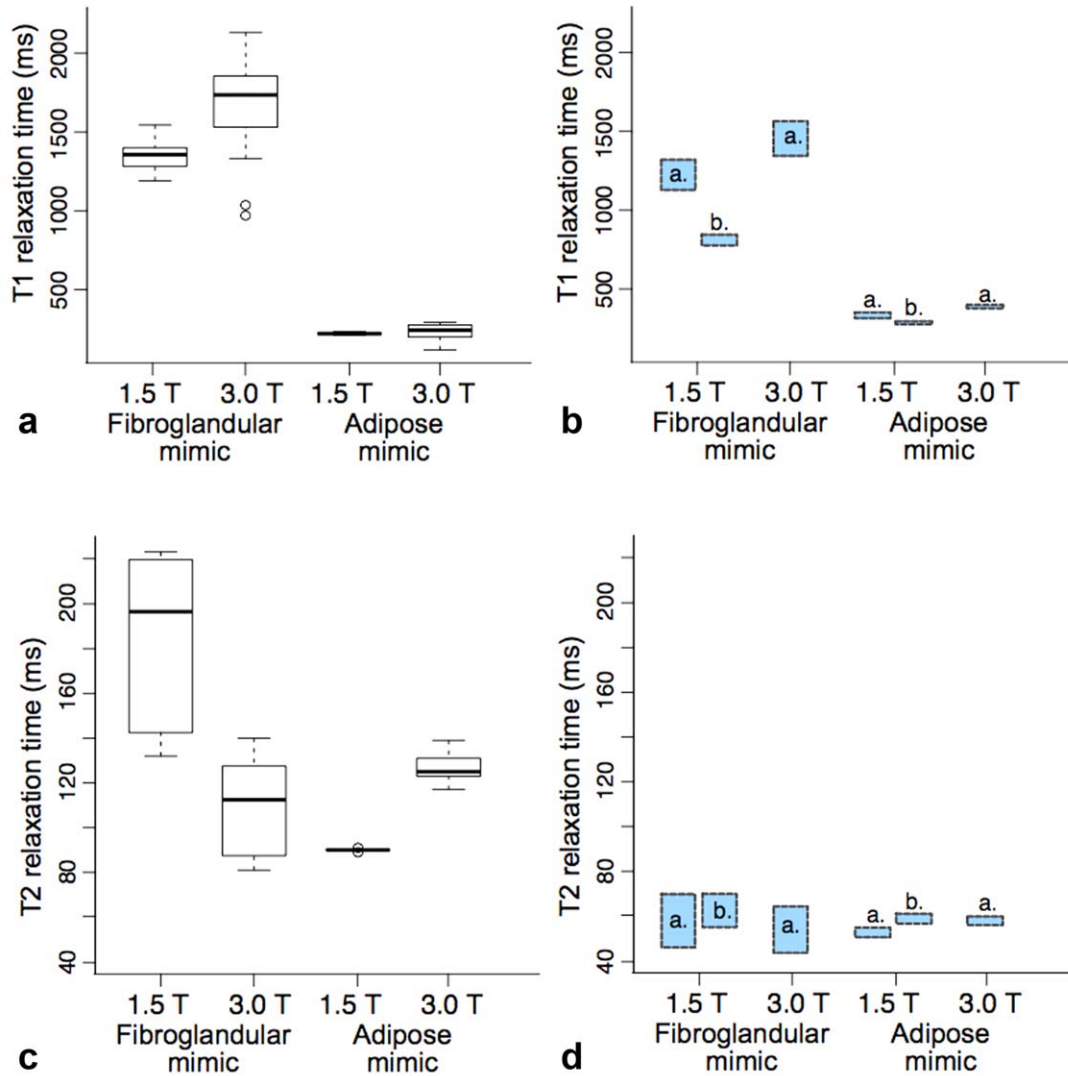


FIGURE 4: The  $T_1$  relaxation times (A) and  $T_2$  relaxation times (C) of the fibroglandular and adipose tissue mimics measured on clinical systems at 1.5T and 3.0T. The target value ranges based on in vivo measurements from the literature (a: Rakow-Penner et al.<sup>10</sup> and b: Merchant et al.<sup>8</sup> are shown for  $T_1$  relaxation (B) and  $T_2$  relaxation (D).

### Clinical Imaging Assessment

The  $T_1$  values of the fibroglandular mimic material measured with the 3D VFA method were slightly higher than the targeted in vivo  $T_1$  values at 1.5T and 3.0T (Fig. 4A), and they were higher than the IR-measured  $T_1$  reference values (1.5T:  $1141 \pm 46$  msec, 3.0T:  $1230 \pm 34.6$  msec). The  $T_2$  relaxation times measured at 1.5T and 3.0T (Fig. 4B) were much longer than the targeted in vivo  $T_2$  time of 54 to 63 msec. The grapeseed oil  $T_1$  measured with the 3D VFA method at 1.5T and 3.0T (Fig. 4A) were just below the IR-measured reference  $T_1$  values (1.5T:  $236 \pm 42$  msec, 3.0T:  $297 \pm 6.3$  msec). The grapeseed oil  $T_2$  relaxation times measured at 1.5T and 3.0T (Fig. 4B) were much longer than the targeted in vivo  $T_2$  time of 53 msec.

The PVP samples in the diffusion phantom closely approximated the range of ADC values from malignant tumors to normal breast tissue (Fig. 5). ADC measurements of PVP were consistent across the MRI system/breast coil

configurations tested and matched the range of ADC reference measurements. Representative diffusion-weighted images and ADC map are shown in Fig. 6.

At 1.5T, the bore temperature ranged from 17 to 18°C, and at 3.0T the bore temperature ranged from 21 to 24°C.

As designed, image distortions can be assessed using the rigid geometry components, especially the regularly spaced grid in the center of the diffusion phantom side. For example, in Fig. 7, which shows computer aided design (CAD) drawings (A,B) and diffusion-weighted images (C,D) of the phantom, the  $T_1/T_2$  unit located on the left side of the coil (C) appears wider than the CAD drawing (A), and the diffusion unit located on the right side of the coil (D), appears narrower than the CAD drawing (B) for that particular configuration of the phantom units. The geometric distortion array has center-to-center spacing 20 mm in the horizontal and vertical directions; we measured the

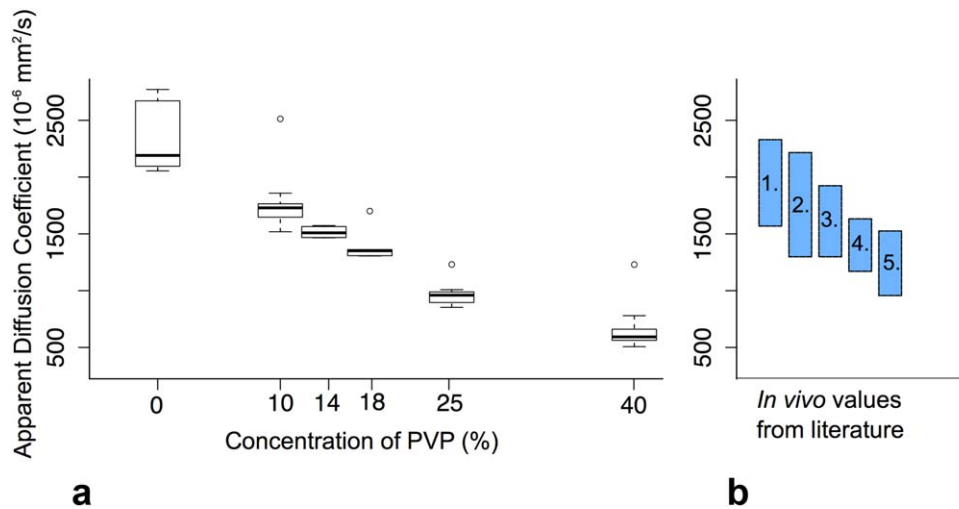


**FIGURE 5:** The ADC of (A) the diffusion mimics measured on clinical 1.5T and 3.0T systems at bore temperature span the range of in vivo values for malignant tumor to healthy tissue (B), as measured in the literature<sup>9,11</sup>: 1. Healthy tissue; 2. Benign mass; 3. Benign lesion; 4. Malignant lesion; and 5. Malignant mass. (A) The measured 25–75 percentile ranges are: 0% PVP: 2140 to 2612  $\times 10^{-6} \text{ mm}^2/\text{s}$ ; 10% PVP: 1689 to 1802  $\times 10^{-6} \text{ mm}^2/\text{s}$ ; 14% PVP: 1516 to 1593  $\times 10^{-6} \text{ mm}^2/\text{s}$ ; 18% PVP: 1358 to 1400  $\times 10^{-6} \text{ mm}^2/\text{s}$ ; 25% PVP: 937 to 1028  $\times 10^{-6} \text{ mm}^2/\text{s}$ ; 40% PVP: 606 to 695  $\times 10^{-6} \text{ mm}^2/\text{s}$ .

horizontal (R/L) center-to-center distances to be 19 mm in Fig. 7D. The vertical (A/P) center-to-center distances in Fig. 7D were 20 mm, as in the CAD drawing.

**Discussion**

In this study a phantom was designed, evaluated, and characterized for quantitative multiparametric MRI studies of the breast. The breast phantom can be used to test fat suppression techniques; mimics  $T_1$  and ADC values measured in vivo; allows comparison testing of the left and right sides of the coil; and can be used to measure image distortion. Ideally, this breast phantom will be a tool to assess system-to-system variability, coil variability, longitudinal variation,<sup>4,6</sup> and variability across sequences, e.g., when evaluating imaging protocols for a clinical trial. This breast phantom allows users to optimize clinical imaging protocols without additional accrual of volunteers or patients.

The phantom design presented here sought to balance the competing goals of minimizing cost and complexity and maximizing functionality. A phantom with additional features could be useful in multiple clinical settings, but such a phantom would be prohibitively expensive, limiting widespread adoption. Hence, several compromises were made to arrive at a cost-effective phantom with clinically relevant imaging features. These compromises included: reducing the number of intended compartments (spheres in the  $T_1/T_2$  phantom unit and tubes in the diffusion phantom unit), using readily available containers and materials when possible, and the ability to position the phantom units on each side of the coil. The breast phantom outer shell is flexible, and the phantom unit position can be adjusted in the medial/lateral plane. These design choices allowed the breast phantom to physically fit into MRI breast coils from two major vendors, which are representative of the commercially available breast coils. This is an improvement over a

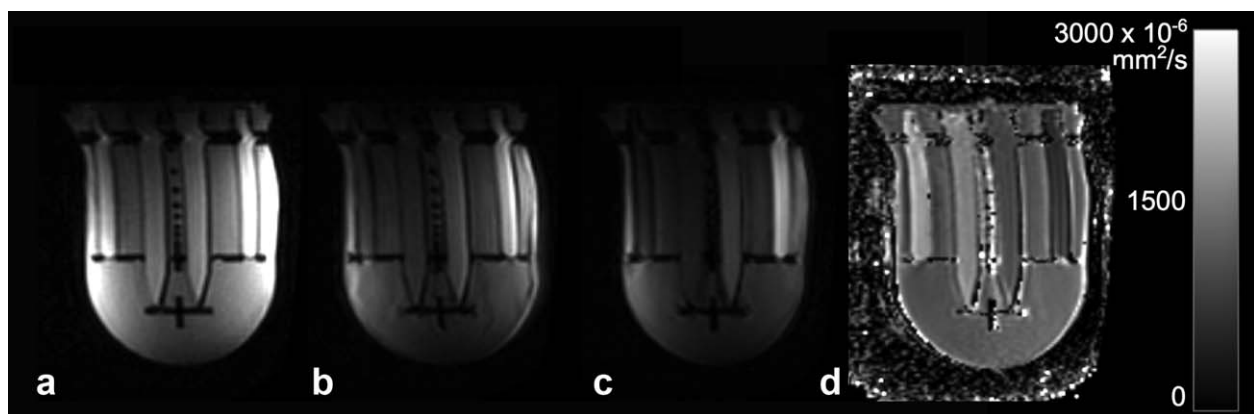


**FIGURE 6:** (A–C) Representative diffusion-weighted images ( $b = 100, 600, 800 \text{ s}/\text{mm}^2$ ) and (D) corresponding ADC map measured on the 1.5T system. The range of ADC values in the phantom (D) covers the range of in vivo ADC values reported in the literature.

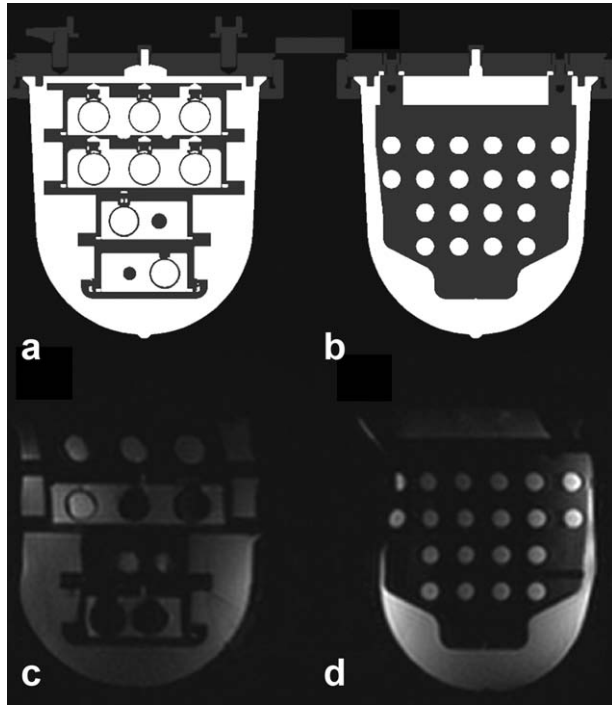


**FIGURE 7:** Comparison of MR representation of the CAD drawing (A,B) and diffusion-weighted image (C,D) of the breast phantom. In the diffusion-weighted image, the  $T_1/T_2$  phantom unit located on the left side of the coil (C) appears wider than the diffusion phantom unit located on the right side of the coil (D), while they are physically the same size, as demonstrated by the CAD drawing (A,B, respectively). In the geometric distortion plate (D), the centers of the regularly spaced array appear narrower in the horizontal direction of the diffusion-weighted image compared to the CAD (B). We measured the horizontal (R/L) center-to-center distances to be 19 mm in (D); the physical spacing is actually 20 mm.

previous breast phantom, which fits in the coil of only one vendor.<sup>6</sup>

Unlike previous breast phantoms,<sup>6,7</sup> this phantom incorporates diffusion mimics. One challenge in developing the diffusion phantom unit was selecting appropriate materials that at bore temperature exhibit the range of ADC values reported in the literature for normal and diseased breast tissue *in vivo*.<sup>9,11</sup> Here, water doped with PVP was used to achieve ADC values ranging from  $600 \times 10^{-6} \text{ mm}^2/\text{s}$  to  $2121 \times 10^{-6} \text{ mm}^2/\text{s}$  in the phantom at bore temperatures, simulating the range of ADC values reported in the literature for malignant lesions and normal tissues.

Another challenge was selection of an appropriate fat mimic to allow for testing the efficacy of different fat saturation techniques frequently used for  $T_1$ -weighted dynamic contrast-enhanced (DCE) MRI and required for diffusion-weighted MRI of the breast. Several options were tested, including separate materials to mimic the  $T_1$  relaxation time of fat tissue (doped water) and the chemical shift from water (various oils). To reduce complexity, grapeseed oil was used because it simultaneously mimicked both the  $T_1$  relaxation time and chemical shift properties of fat. The signal

from the silicone outer shell provided an additional opportunity to assess spectral fat suppression.

The modular design of the breast phantom is advantageous, in particular to the research community, as it will allow customization and reconfiguration to address concerns in breast MRI beyond the  $T_1$  and diffusion characterization reported here. The spheres on the  $T_1$  phantom unit are attached via plastic screws and could be swapped for spheres containing other materials. Similarly, the tubes on the diffusion side can be easily removed and replaced with other tubes. Future investigations could include the introduction of mimics for microcalcifications, cysts, the presence of biopsy clips, and silicone breast implants. Such modularity is one of several factors that make this breast phantom a robust platform for clinical imaging development, testing, optimization, and quality assurance.

The current phantom design is not without limitations. While the design enables heterogeneous distribution of the fibroglandular and adipose mimic materials suitable for testing of fat suppression, one limitation is that the physical separation between fibroglandular tissue and adipose tissue is not present in the human breast. To ensure consistent distribution of the fibroglandular and adipose mimic materials while maintaining the stability of these materials, it is best to confine the mimics to sealed containers. The containers in this phantom, made of polycarbonate material, add a separation between fibroglandular and adipose tissue mimics that does not exist in the body. In addition, these containers can contribute susceptibility artifacts and echo-planar imaging artifacts. In its current design, the breast phantom does not possess a mechanism for temperature control or tracking, which is necessary to determine the accuracy of ADC measurements. Another limitation of the current phantom design is that the fibroglandular mimic (35% w/w corn syrup)  $T_2$  relaxation time varies greatly with magnetic field strength. This is not consistent with properties of breast tissue observed *in vivo*, where the  $T_2$  relaxation time is independent of field strength.<sup>10</sup> Until a more suitable fibroglandular mimic is found, we do not recommend using the breast phantom for  $T_2$  measurements. Finally, over the course of several months the fibroglandular mimic (35% w/w corn syrup) was susceptible to bacterial growth when in contact with the silicone shell; this may affect the stability of relaxation properties.

Future designs of the breast phantom will include several revisions to address the identified limitations and to improve the phantom's utility. One such improvement is the capability to assess contrast-enhanced measurements. Typical  $T_1$  measurements in the breast are contrast-enhanced with gadolinium; hence, it is worth considering the inclusion of a dynamic contrast component similar to that used by Freed et al.<sup>7</sup> in the next iteration of the phantom. In addition, an alternative adipose tissue mimic will be explored. Natural

oils typically demonstrate subtle batch-to-batch variation in properties, making them less than ideal for environments in which both precision and accuracy are essential. Hence, it will be necessary to explore alternative adipose tissue mimics, preferably a synthetic oil, which is shelf-stable and consistent across production batches. However, oil selection is complicated by the requirement that the oil used should ideally mimic both the  $T_1$  relaxation time and the chemical shift observed in adipose breast tissue (synthetic mineral oils tested thus far do not possess a long enough  $T_1$ ). To date, aqueous paramagnetic salt solutions and PVP solutions show excellent stability (results not shown).

In conclusion, we designed a breast phantom that can be used to validate MRI clinical trial sites and for quality control, specifically  $T_1$  relaxation time and ADC measurements. Despite the highlighted limitations, the phantom met the goals of clinically relevant values for breast tissue  $T_1$  and ADC and can be used to test clinical protocols. Additionally, the phantom can be used to examine other imaging challenges common to breast MRI. For example, the phantom could be used to assess the quality of the fat suppression technique, EPI distortion artifacts, which are dependent on the phase-encoding direction, gradient nonlinearity effects,<sup>21</sup> especially along the long axis of the tubes in the diffusion phantom unit, and measurement variability due to the selected b-values.<sup>22</sup> The breast phantom has long-term support from a national metrology institute, which is a benefit for clinical trials using quantitative MRI.

## Acknowledgments

Contract grant sponsor: National Research Council postdoctoral scholarship; contract grant number: NIH/NCI 1U01CA151235

The authors thank Ms. Evelyn Proctor for assistance scanning the phantom. Contribution of the National Institute of Standards and Technology; not subject to copyright in the United States. Certain commercial instruments and software are identified to specify the experimental study adequately. This does not imply endorsement by NIST or that the instruments and software are the best available for the purpose.

## References

1. Cancer Among Women: Division of Cancer Prevention and Control, Centers for Disease Control and Prevention; 2015 [updated August 20, 2015; cited 2015 November 10, 2015]. Available from: <http://www.cdc.gov/cancer/dpcp/data/women.htm>.
2. Barker AD, Sigman CC, Kelloff GJ, Hylton NM, Berry DA, Esserman LJ. I-SPY 2: an adaptive breast cancer trial design in the setting of neoadjuvant chemotherapy. *Clin Pharmacol Ther* 2009;86:97–100.
3. Turnbull L, Brown S, Harvey I, et al. Comparative effectiveness of MRI in breast cancer (COMICE) trial: a randomised controlled trial. *Lancet* 2010;375:563–571.
4. Glover GH, Mueller BA, Turner JA, et al. Function biomedical informatics research network recommendations for prospective multicenter functional MRI studies. *J Magn Reson Imaging* 2012;36:39–54.
5. Mazzara GP, Briggs RW, Wu Z, Steinbach BG. Use of a modified polysaccharide gel in developing a realistic breast phantom for MRI. *Magn Reson Imaging* 1996;14:639–648.
6. Tuong B, Gardiner I. Development of a novel breast MRI phantom for quality control. *AJR Am J Roentgenology* 2013;201:W511–515.
7. Freed M, de Zwart JA, Loud JT, et al. An anthropomorphic phantom for quantitative evaluation of breast MRI. *Med Phys* 2011;38:743–753.
8. Merchant TE, Thelissen GR, de Graaf PW, et al. Application of a mixed imaging sequence for MR imaging characterization of human breast disease. *Acta Radiol* 1993;34:356–361.
9. Partridge SC, Mullins CD, Kurland BF, et al. Apparent diffusion coefficient values for discriminating benign and malignant breast MRI lesions: effects of lesion type and size. *AJR Am J Roentgenol* 2010;194:1664–1673.
10. Rakow-Penner R, Daniel B, Yu H, Sawyer-Glover A, Glover GH. Relaxation times of breast tissue at 1.5T and 3T measured using IDEAL. *J Magn Reson Imaging* 2006;23:87–91.
11. Partridge SC, Demartini WB, Kurland BF, Eby PR, White SW, Lehman CD. Differential diagnosis of mammographically and clinically occult breast lesions on diffusion-weighted MRI. *J Magn Reson Imaging* 2010;31:562–570.
12. Horkay F, Pierpaoli C, Basser PJ. Phantom for diffusion MRI imaging. USA patent no. US 20120068699 A1, 2012.
13. Pierpaoli C, Sarlls J, Nevo U, Basser PJ, Horkay F. Polyvinylpyrrolidone (PVP) water solutions as isotropic phantoms for diffusion MRI studies. In: Proc 17th Meeting ISMRM, Honolulu; 2009.
14. Russek SE, Boss MA, Jackson EF, et al. Characterization of NIST/ISMRM MRI system phantom. In: Proc 20th Meeting ISMRM, Melbourne; 2012.
15. Newville M, Stensitzki T, Allen DB, Ingargiola A. LMFIT: non-linear least-square minimization and curve-fitting for Python. Zenodo (open access software) 2014.
16. Hahn EL. An accurate nuclear magnetic resonance method for measuring spin-lattice relaxation times. *Phys Rev* 1949;76:145–146.
17. Meiboom S, Gill D. Modified spin-echo method for measuring nuclear relaxation times. *Rev Sci Instrum* 1958;29:688–691.
18. Partridge SC, Heumann EJ, Hylton NM. Semi-automated analysis for MRI of breast tumors. *Studies Health Technol Inform* 1999;62:259–260.
19. Deoni SC, Rutt BK, Peters TM. Rapid combined T1 and T2 mapping using gradient recalled acquisition in the steady state. *Magn Reson Med* 2003;49:515–526.
20. Wang HZ, Riederer SJ, Lee JN. Optimizing the precision in T1 relaxation estimation using limited flip angles. *Magn Reson Med* 1987;5:399–416.
21. Newitt DC, Tan ET, Wilmes LJ, et al. Gradient nonlinearity correction to improve apparent diffusion coefficient accuracy and standardization in the american college of radiology imaging network 6698 breast cancer trial. *J Magn Reson Imaging* 2015;42:908–919.
22. Partridge SC, Murthy RS, Ziadloo A, White SW, Allison KH, Lehman CD. Diffusion tensor magnetic resonance imaging of the normal breast. *Magn Reson Imaging* 2010;28:320–328.